JOURNAL OF GEOPHYSICAL RESEARCH, VOL. 104, NO. B9, PAGES 20,431–20,447, SEPTEMBER 10, 1999

Crustal structure beneath the central Oregon convergent margin from potential-field modeling: Evidence for a buried basement ridge in local contact with a seaward dipping backstop

Sean W. Fleming[1] and Anne M. Tréhu
College of Oceanic and Atmospheric Sciences, Oregon State University, Corvallis

Abstract. Models of magnetic and gravity anomalies along two E-W transects offshore central Oregon, one of which is coincident with a detailed velocity model, provide quantitative limits on the structure of the subducting oceanic crust and the crystalline backstop. The models indicate that the backstop-forming western edge of the Siletz terrane, an oceanic plateau that was accreted to North America ~50 million years ago, has a seaward dip of less than 60°3. Seismic, magnetic, and gravity data are compatible with no more than 2 km of subducted sediments between the Siletz terrane and the underlying crystalline crust of the Juan de Fuca plate. The data also suggest the presence of a N-S trending, 200-km-long basaltic ridge buried beneath the accretionary complex from about 43°N to 45°N. Although the height and width of this ridge probably vary along strike, it may be up to 4 km high and several kilometers wide in places and appears to be locally in contact with the Siletz terrane beneath Heceta Bank. Several models for the origin of this ridge are discussed. These include: a sliver of Siletz terrane detached from the main Siletz terrane during a late Eocene episode of strike-slip faulting; imbrication and thickening of subducted oceanic crust in place; an aseismic ridge rafted in on the subducting oceanic crust during the past 1.2 million years; and a series of ridges and/or seamounts rafted in over a longer period of time and transferred from the subducting plate to the overlying plate. The last model is the most consistent with the complicated history of local uplift, subsidence, and slope instability recorded in the ridges, basins, and banks of this part of the margin. We speculate that the massive seaward dipping western edge of the Siletz terrane in this region inhibits subduction of seamounts and sediments, resulting in fomation of buried ridge as the accumulated flotsam and jetsom of subduction. This process may also be responsible for thickening of lower accretionary complex material, oversteepening of slopes leading to massive slumping, and north-south extension through strike-slip faulting in the accretionary complex to the west of the buried ridge. Regardless of its origin, the ridge may currently be acting as an asperity inhibiting subduction.

1. Introduction

Subduction of the Juan de Fuca plate beneath northern California, Oregon, Washington, and British Columbia has produced a geologically complex convergent margin (Figure 1a). The distribution of seismic activity, however, is unusual for this tectonic setting. Although great interplate earthquakes have occurred during the Holocene [*Nelson et al.*, 1995], interplate seismicity is almost absent from the historical record, and the distribution of both upper and lower plate seismicity is very heterogeneous (Figures 1b and 1c). Earthquake activity is common in Washington and northern California [e.g., *Weaver and Shedlock*, 1996] but is infrequent in central and southern Oregon. In Washington the high level of seismic activity may result from northward motion of a Paleocene to early Eocene accreted basaltic terrane generally referred to as the Siletz terrane [*Snavely et al.*, 1968] relative to pre-Tertiary North America [*Wells et al.*, 1998]; here forearcseismicity generally outlines blocks of Siletz terrane [*Tréhu et al.*, 1994; *Parsons et al.*, 1998]. In northern California, seismicity in both the upper and lower plates seems to be controlled in large part by the northward motion of the Pacific plate [*Wang*, 1996]. Understanding the nearly aseismic behavior of both the upper and lower plates of the central part of the subduction zone requires a better understanding of the crustal structure in this region in order to determine whether this is a locked zone with the potential for great earthquakes or simply a node in the regional stress regime.

To this end, we have modeled marine magnetic and gravity anomaly data recorded along two E-W profiles. The original goals of this study were to (1) use potential-field data to regionally extend constraints on crustal structure obtained from a previous seismic reflection-refraction survey (Figure 1d); (2) constrain the geometry of the backstop-forming western edge of the Siletz terrane; (3) constrain the structure beneath Heceta Bank, a shallow submarine bank on the central Oregon margin; and (4) evaluate the influence of backstop structure on deformation in the accretionary complex. In the course of this work, we also identified a previously unknown, deeply buried basement ridge on the subducting plate, which provides a possible explanation for the complicated geologic history of

[1]Now at Duncan, British Columbia, Canada.

Paper number 1999JB900159.
0148-0227/99/1999JB900159$09.00

this part of the margin and which may currently be acting as an asperity between the plates.

1.1. The Siletz Terrane

The thick basalts of the Siletz terrane form the backstop to the accretionary complex on the central Oregon continental margin. A backstop may be defined as a region within a forearc that has significantly greater shear strength than trenchward sediments and which thus acts as a bulldozer blade driving the accretionary wedge [*Davis et al.*, 1983; *Wang and Davis*, 1996]. Differing backstop geometries produce different stress and strain fields within an accretionary prism [*Byrne et al.*, 1993], and the dynamics of sediment subduction, melange formation, and prism accretion are in part a function of the geometry and properties of the backstop

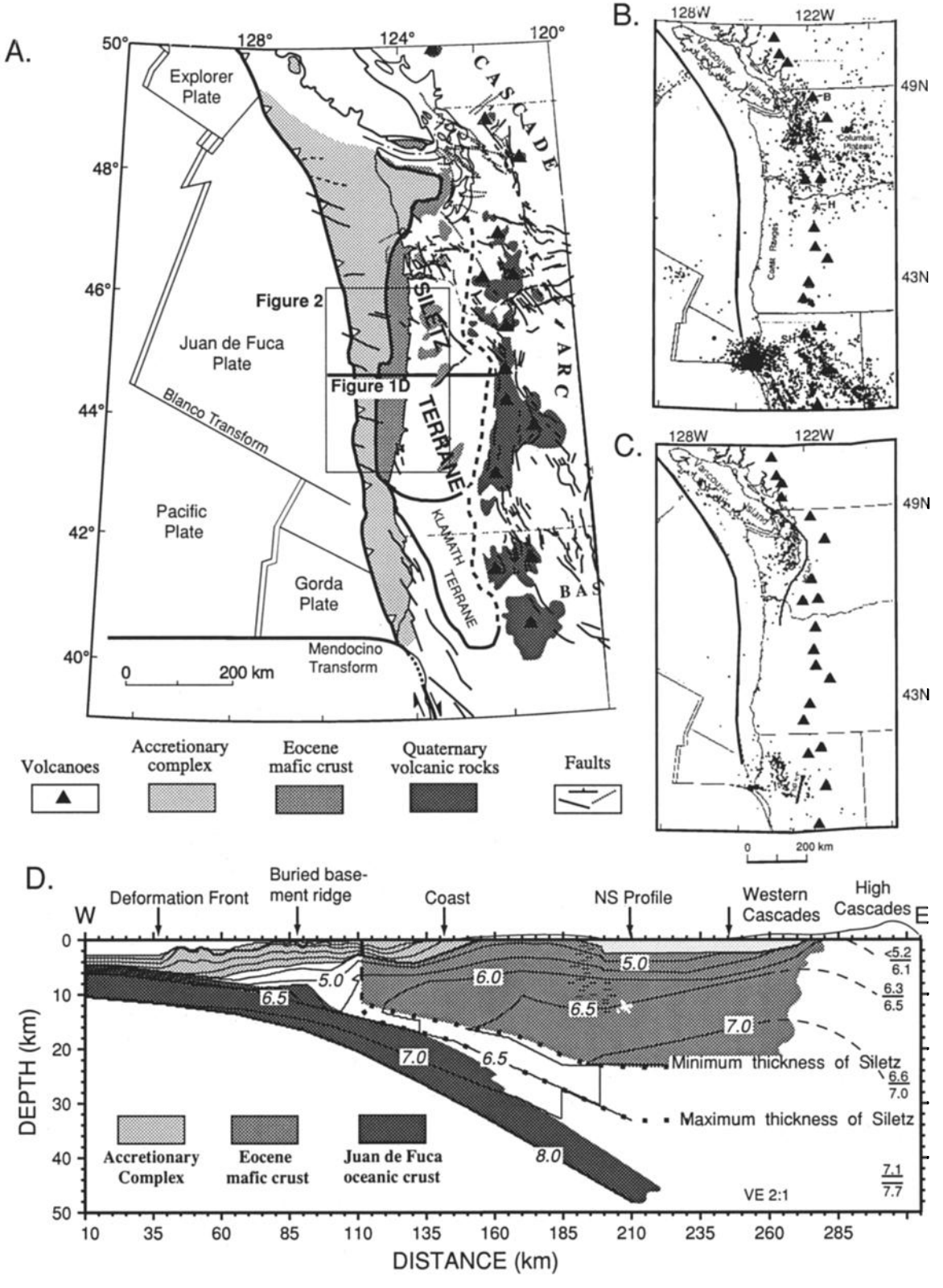

[*Shrieve and Cloos*, 1986; *von Huene et al.*, 1996]. The geometry of the backstop thus helps to determine subduction zone dynamics and is an important consideration in earthquake hazard assessment. Thermal models of the Cascadia subduction zone are also sensitive to the geometry and extent of the low thermal conductivity basalts of the Siletz terrane (*Hyndman and Wang*, 1993; *Oleskevich*, 1994), and these models are critical for predicting the size of the locked zone and thus the magnitude of a possible megathrust earthquake.

The rocks of the Siletz terrane are tholeiitic submarine pillow lavas and breccias which grade locally into subaerially erupted alkalic basalts [*Snavely et al.*, 1968; *Simpson and Cox*, 1977; *Duncan*, 1982], and they are locally known as the Siletz River Volcanics in Oregon, the Crescent Formation in Washington, and the Metchosin Volcanics in British Columbia. Seismic data indicate large variations in the thickness of this terrane. Its thickness is greatest beneath west central Oregon [*Tréhu et al.*, 1994], where it reaches 24-32 km (Figure 1d) and the velocity structure resembles that of the Ontong Java plateau and other large igneous provinces [*Hussong et al.*, 1979; *Coffin and Eldholm*, 1993]. It thins to ~20 km beneath northwestern Oregon and southwest Washington [*Tréhu et al.*, 1994; *Parsons et al.*, 1998] and has approximately the same thickness as normal oceanic crust where it is thrust beneath the pre-Tertiary terranes of Vancouver Island [*Hyndman*, 1995]. Several investigators [*Wells et al.*, 1984; *Trehu et al.*, 1994; *Parsons et al.*, 1998; *Wells et al.*, 1998] have suggested that these variations have influenced long- and short-term forearc deformation, with the thickest part of the terrane acting as a coherent rotating block that deflects seismic and aseismic deformation to its edges. The gravity anomaly data (Figure 2a) reflect the presence of dense Siletz rocks near the surface beneath the Coast Range data but are of limited use in mapping the boundaries of this terrane because the signal is overprinted by gravity lows associated with shelf basins to the west and the Willamette Valley to the east.

The magnetic anomaly data (Figure 2b) and drill holes [*Snavely*, 1987; *Snavely and Wells*, 1996], on the other hand, clearly show that the western edge of the Siletz terrane lies beneath the continental shelf of central Oregon between 43°N and 45°N. *Snavely et al.* [1980] suggested that this boundary, which they named the Fulmar fault, was a right-lateral strike-slip fault during the Eocene that truncated the accreted Siletz terrane. Although this boundary is currently aseismic, several observations suggest that it separates regions with different stress regimes and deformational styles and that it has been the site of Neogene deformation [*Snavely et al.*, 1980; *Tréhu et al.*, 1995] (see also Figure 3). Both the N-S strike of ubiquitous anticlines and thrust faults and the northwest strike of active left-lateral strike-slip faults in the accretionary complex offshore Oregon indicate that the maximum horizontal compressive stress is generally oriented E-W seaward of the backstop [*Goldfinger et al.*, 1992, 1997]. In contrast, the orientation of maximum horizontal compressive stress in the onshore forearc is N-S [*Werner et al.*, 1991; *Ludwin et al.*, 1991]. Moreover, northwest trending, left-lateral strike-slip faults that are common in the accretionary prism appear to terminate eastward near the seaward edge of the Siletz terrane [*Goldfinger et al.*, 1997]. Finally, a band of short-wavelength (3-4 km) margin-parallel folds and faults, which contrasts sharply with longer-wavelength (6-8 km) folds that occur throughout the rest of the accretionary complex, overlies this boundary in the region of this study. Stonewall Bank, an actively growing anticline that has recently been studied in detail by *Yeats et al.* [1998], may be a particularly well-developed example of one of these folds.

1.2. Heceta Bank

The short-wavelength folds overlying the apparent seaward edge of the Siletz terrane are particularly prominent over Heceta Bank (C. Hutto, personal communication, 1996), an enigmatic bathymetric high located at approximately 44°00'N to 44°30'N and extending westward on the continental shelf to about 125°00'W (Figures 2a and 2b). Although the bank is associated with a large (~50 mGal) free-air gravity high (Figure 2a), the simple spatial correlation between gravitational and bathymetric anomalies that would be expected if the gravity field reflected only topography and large-scale plate geometry is not observed. Magnetic data suggest that the Siletz terrane does not extend sufficiently far west to entirely underlie Heceta Bank (Figure 2b).

Heceta Bank and other banks of the central Cascadia margin have been interpreted to be an outer arc high formed by underthrusting of young sediments at the base of the accretionary complex [*Kulm and Fowler*, 1974]. However, it remains poorly understood why the outer arc high exists as a number of discrete banks rather than as a continuous bathymetric and structural feature along the entire margin. Recent regional mapping of the Miocene-Pliocene unconformity suggests that the outer arc high was once more extensive, extending north of Heceta Bank to 46°N beneath what is now the continental slope, suggesting post-Miocene collapse of the margin through gravitational collapse and/or subduction erosion [*McNeill et al.*, 1998].

Figure 1. (a) Generalized geological and tectonic map of the Cascadia subduction zone, showing plate boundaries, Quaternary volcanic rocks of the present arc, Eocene mafic crust of the Siletz terrane in the forearc (exposed on land, and inferred offshore), and crustal faults. Map is modified from *Wells et al.* [1998], with additional offshore faults from *Goldfinger et al.* [1997]. The locations of the cross-section of Figure 1d and of the potential field maps of Figure 2 are also shown. (b) Earthquakes with hypocenters shallower than 30 km from 1980 to September 1993 [from *Weaver and Shedlock*, 1996]. Except for near the Mendocino triple junction and in the ocean basin, these events are in the North American plate. (c) Earthquakes with hypocenters deeper than 30 km from 1980 to September 1993 [from *Weaver and Shedlock*, 1996]. These events are in the subducting Juan de Fuca/Gorda plate. Note the lack of seismic activity in either plate beneath central Oregon. (d) Velocity model for a transect across the Cascadia forearc in central Oregon. [Reprinted with permission from *Tréhu et al.*, 1994. Copyright 1994 American Association for the Advancement of Science.] Velocity contours are labeled in km/s. This model provided a starting point for the potential-field modeling of the northern line. The model was derived from an offshore multichannel seismic profile, which was also recorded on ocean bottom and onshore seismometers, and from several onshore refraction profiles. The seaward extent of the Siletz terrane is indicated by a sharp lateral change in velocity near km 110.

2. Data

The prominent gravity highs beneath the Oregon Coast Range (Figure 2a) are interpreted to be uplifted Siletz River Volcanics exposed in the Oregon Coast Range [*Bromery and Snavely*, 1964; *Snavely et al.*, 1980; *Snavely*, 1987]. On a regional scale, these anomalies express the excess mass of the Siletz terrane within the forearc [*Wells et al.*, 1998], consistent with its anomalous thickness measured seismically [*Tréhu et al.*, 1994]. The edges of the anomaly, however, are affected by the burial of the Siletz terrane beneath sedimentary rocks of continental shelf basins and the Willamette Valley, and these edges do not precisely map the boundaries of the terrane. West of 125°, the gravity data reflect the eastward dip of the subducting Juan de Fuca plate and low-density trench fill sediments, as is typical of subduction zones. Between the "trench" and the Coast Range gravity highs, the data reflect a complex interplay between seafloor topography, changing depth to the Juan de Fuca plate, the internal density structure of the accretionary prism, the edge of crystalline continental basement, and the distribution of a number of small, shallow basins filled with unconsolidated sediments.

The magnetic data have been used to qualitatively locate the seaward edge of crystalline basement offshore where it is juxtaposed against the accretionary complex [*Bromery and Snavely*, 1964; *Snavely et al.*, 1980; *Snavely*, 1987]. This determination is generally in agreement with that determined on a seismic cross section [*Tréhu et al.*, 1994, 1995]. Changes in the gradient at the western edge of this anomaly suggest variation in the shape of this boundary, assuming a simple mag-

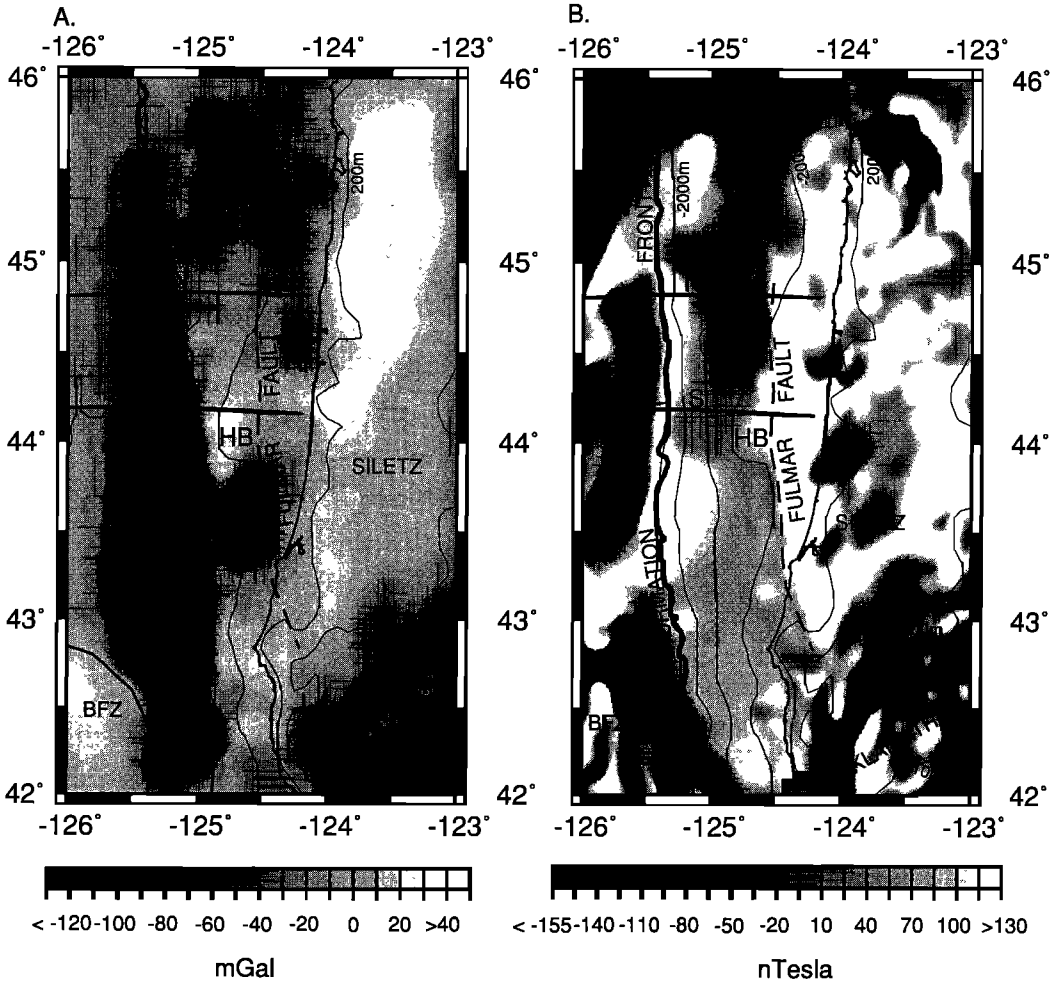

Figure 2. (a) Gravity anomalies of the central Oregon continental margin from the *Geophysics of North America, CD-ROM version 1 0* [1987]. Bouguer gravity is shown onshore; free-air gravity is shown offshore. Corrections and gridding algorithms used to construct this data set are described by *Godson and Scheibe* [1982]. Two east-west trending lines labeled N and S on both maps show the locations of the two shipboard profiles that were modeled for this paper. The coastline, deformation front, and Blanco fracture zone (BFZ) are shown as black lines. The Fulmar fault of *Snavely et al.* [1980] is shown as a dashed line. Thin black lines are topographic contours indicating depths of 200, 1000, and 2000 m offshore and elevations of 200, 600 and 1000 m onshore. HB, Heceta Bank; NB, Nehalem Bank. (b) Magnetic anomalies of the central Oregon continental margin from the Geophysics of North America CD-ROM. The original source for the data from the Oregon continental margin is a series of aeromagnetic surveys flown at an elevation of about 500 ft ground clearance and 1.6-8 km mile line spacing [U.S. Geol. Surv., 1970]. Data were regridded to correspond to the gravity grid as described by *Godson* [1987]. Overlays are the same as those for Figure 2a.

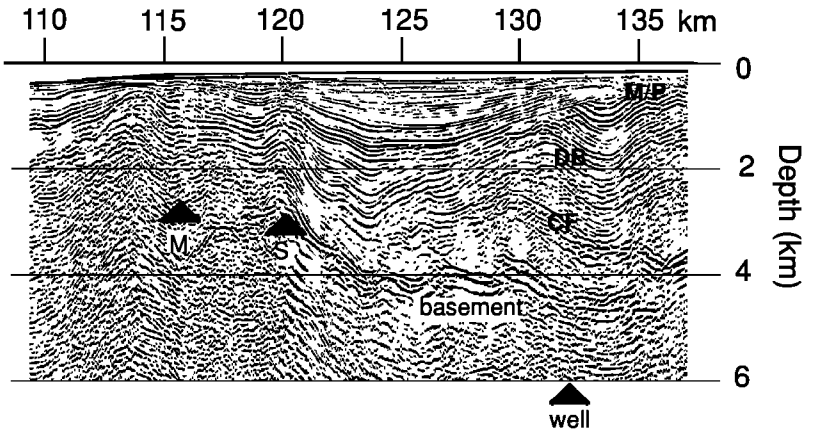

Figure 3. Migrated, depth-converted detail of the seismic profile of *Tréhu et al.* [1995] across the central Oregon continental margin. The reflection identified as the top of Siletz is shown (labeled basement), as is the western extension of this terrane into a region of discontinuous diffractions that is required to model the magnetic anomaly data. S marks the seaward edge of the Siletz terrane as identified on the seismic data; M is the seaward edge based on magnetic modeling. M/P is the Miocene/Pliocene unconformity. The position of an industry test well, in which two Miocene sills (labeled DB, and CF) were encountered, is also marked. The short-wavelength folds and possible recent fault overlying the region between km 115 and 120 are characteristic of a narrow band of folds and faults that overlie the seaward edge of the Siletz terrane.

netization contrast. Onshore, the magnetic data are quite variable and generally reflect outcrop patterns of the Siletz volcanics and of localized and variably magnetized upper Eocene and Miocene basalts [e.g., *Bromery and Snavely*, 1964; *Simpson and Cox*, 1977]. Near the deformation front the magnetic lineations in this region have been identified as seafloor spreading anomalies 4 and 4a [*Wilson*, 1993]. Between 125° and the edge of the Siletz terrane, the magnetic data show a "quiet zone."

Although the gridded potential-field data define general patterns, they have been smoothed considerably. We therefore examined shipboard data from 43°00'N to 46°00'N that were acquired independently by a number of agencies and universities [*Marine Trackline Geophysics CD-ROM, version 3.2*, 1996]. Data are generally consistent from cruise to cruise. Shipboard data acquired by the National Oceanographic and Atmospheric Administration (NOAA) were selected for the modeling procedure because magnetic, free-air gravity, and bathymetry data were collected simultaneously, the ship tracks were oriented approximately perpendicular to the predominant N-S geological strike, and the survey lines were of the greatest spatial density. The data were resampled using an Akima spline with a 0.5-km sampling interval prior to modeling.

The first profile modeled is approximately coincident with the seismic model of *Tréhu et al.* [1994]. For this profile we focus on modeling the magnetic data and show that the gravity data are compatible with this model. A second profile crossing Heceta Bank was chosen for modeling because it represents a distinct contrast in margin morphology and the slope of the magnetic anomaly marking the seaward edge of the Siletz terrane. For this profile we show that the magnetic model is consistent with conclusions obtained from modeling line 1, and we focus on modeling the gravity data. Models for these two profiles should bracket the range of structure along this central segment of the Cascadia margin.

3. Modeling: North Line

We used gravity and magnetics modeling software produced by Northwest Geophysical Associates (Corvallis, Oregon), which is based on the algorithms of *Talwani et al.* [1959] and *Talwani and Heirtzler* [1964] and incorporates the algorithm of *Webring* [1985] for least squares inversion of selected model parameters. Because the large-scale geometry of the Oregon continental margin consistently strikes N-S, perpendicular to the survey lines, and because small-scale, three-dimensional variation is poorly constrained, the models discussed here are two-dimensional. We did, however, calculate the effect of the northern and southern termination of Heceta Bank on modeled gravity anomalies and determined that three-dimensional effects were not significant. Because of multiple trade-offs among various parameters, multiple starting models were considered, and a hybrid forward-inverse approach was adopted in which only a single parameter was varied at a time.

3.1. Initial Model Parameterization

The general geometry for the Siletz terrane, Juan de Fuca plate, shelf sediments, and accretionary prism in the seismic model (Figure 1d) was used in our initial potential-field model. Two important features of this model, the basement the western edge of the Siletz terrane, were not included in the initial model, because we wanted to test the existence of these features independently.

Detailed structure of the top of the Siletz terrane was interpreted from USGS multichannel seismic reflection line L376W005 [*Snavely*, 1987], a proprietary industry seismic reflection line, and the seismic reflection line of *Tréhu et al.* [1995] and converted to depth using a velocity of 1.8 km/s for sediments above the Pliocene-Miocene unconformity and 3.0 km/s for sediments below it. Interpretations of well log data [*Peterson et al.*, 1984] and a synthetic seismogram computed

from the sonic logs [*Cranswick and Piper*, 1991] of an industry well generally confirm our interpretation of the seismic reflection data and our velocity estimates. The top surface of the Siletz terrane is imaged offshore in these data sets as a block-faulted reflector to model km ~115 ("S" in Figure 3). West of this location, several discontinuous diffractions are observed, but basement cannot be unambiguously identified.

Two strong reflections, located at ~1.25 and 2.4 s in the vicinity of the well, are observed in the data (DB and CF in Figure 3). Drill hole data suggest that these reflections result from Miocene basalts associated with the onshore Depoe Bay and Cape Foulweather basalts [*Cranswick and Piper*, 1993; *Peterson et al.*, 1984; *Snavely et al.*, 1980]. The extent of these basalts to the north and south is not well constrained, but the seismic reflection data suggest that they terminate at least 10–15 km east of the Siletz terrane's western edge, and drill hole data show that the units are thin [*Snavely et al.*, 1980; *Snavely*, 1987; *Peterson et al.*, 1984]. These Miocene basalts were not explicitly included in the model, because their impact on the overall anomaly is small and their magnetic parameters are poorly constrained.

Starting values for magnetic parameters of the Juan de Fuca plate were a remanent magnetization intensity M_R of ± 0.001 emu/cm^3 (in general agreement with *Finn* [1990] and *Butler* 1992] and a susceptibility K of 0.003 cgs units (in general agreement with *Telford et al.*, 1990). (Note that we cite magnetization properties in cgs units to be consistent with most prior literature. To convert to SI, multiply susceptibility values by 4π and multiply remanent magnetization values by 10^3 to convert emu/cm^3 to A/m). No direct measurements of M_R and K are available for Juan de Fuca plate basalts offshore Oregon, but these initial model values give a reasonable Koenigsberger ratio for oceanic basalt of ~1 and required little subsequent modification to provide a reasonable match to the magnetic data. Inclination I and declination D of the remanent field were set equal to that of the present geomagnetic field (I = 68° and D = 19°) on the assumption that no major crustal rotations of the young Juan de Fuca plate have occurred in the study area [*Finn*, 1990]. This assumption is justified by the observation that seafloor spreading magnetic lineations offshore central Oregon are parallel to the current orientation of the spreading center. Using *Wilson*'s [1993] identification of anomalies 4 (~7.4 Ma) and 4a (~9.1 Ma), we calculated a half-spreading rate of 3.65 cm/yr and projected the magnetic lineations of the subducted oceanic plate downdip using the geomagnetic time-scale of *Cande and Kent* [1992].

The internal stratigraphy of the offshore portion of the Siletz terrane is unknown; therefore this block consists of an unconstrained vertical and horizontal distribution of normal and reverse magnetization polarities and variable M_R and K. However, on the basis of the observed magnetic signature of the Siletz terrane, paleomagnetic data, and other information [*Fleming*, 1996], we were able to make two simplifying assumptions: (1) Bulk M_R for the Siletz terrane may be considered negligible and (2) variations in K within the Siletz terrane are distributed on a much smaller length scale than the crustal scale of the terrane itself and of our crustal-scale model. As magnetic properties commonly vary by orders of magnitude within a single outcrop, this second simplifying assumption is implicitly made in any magnetic modeling effort [e.g., *Finn*, 1990], and allows us to assign a single K value for large crustal blocks.

Densities for our initial model were determined by calculating a best fit polynomial to the well-known Nafe-Drake velocity versus density data (from the RAYINVR seismic modeling program written by C. Zelt and discussed by *Zelt and Smith* [1992], extended to include additional data for crystalline rocks [e.g., *Godfrey et al.*, 1997]. This equation was applied to the gridded velocity model [*Tréhu et al.*, 1994], which contains both lateral and vertical velocity gradients. The resulting gridded density model was then simplified to obtain an initial model parameterized by isodensity blocks.

3.2. Magnetic Model

Assuming K and M_R of 0.003 and +-0.001 for the oceanic crust of the subducted Juan de Fuca plate results in a predicted long-wavelength magnetic high in the magnetic quiet zone (curve IN on Figure 4a). Increasing K and M_R for anomaly 4 to 0.0035 and 0.0015 and then gradually decreasing K and M_R for anomaly 5 to 0.0008 and 0.0001 results in a much better fit to the observed magnetic anomalies west of the Siletz terrane anomaly (curve DEMAG on Figure 4a). We do not attempt to interpret the variability in magnetic properties for anomaly 4 as it is within the uncertainty of our knowledge of the magnetic properties of oceanic crust. The required decrease in magnetization for anomaly 5, however, is significant. Thermal models [*Scheidegger*, 1984; *Hyndman and Wang*, 1993] suggest that the subducting slab is not hot enough to attribute all of the apparent demagnetization to thermal demagnetization, and some chemical demagnetization due to metamorphism is therefore also likely, as discussed in section 5.1.

The next step in the modeling procedure was to add the effect of the Siletz terrane. Because magnetic modeling is most sensitive to the shorter-wavelength response of shallow structure [*Webring*, 1985], we were able to determine through trial and error that the upper surface of the Siletz terrane must extend slightly seaward and upward of the westernmost position where it is clearly imaged in seismic data ("M" in Figure 3) to include a region of diffractions indicative of rough topography. This seaward extension is only weakly sensitive to K. However, the modeled geometry of the edge of the Siletz terrane and its modeled susceptibility are theoretically correlated [*Webring*, 1985], and the sensitivity of modeled geometry to modeled susceptibility must be evaluated when considering the geometry of the entire backstop.

Assuming that the western side of the Siletz terrane is a straight line in cross section, we created 64 models, representing eight values of susceptibility and eight values of dip, holding all other model parameters constant. The root-mean-square error for each model as a function of dip and susceptibility is shown in Figure 5. The best fit dip and susceptibility for this simple model are 55°W and 0.00285 cgs units, respectively. Fit rapidly deteriorates as the dip becomes vertical or landward (>90°). Curve ST in Figure 4a shows the effect of adding the Siletz terrane to the model with these parameters. This value for K is consistent with values measured by *Bromery and Snavely* [1964] for samples of Siletz rocks from western Oregon. Implications of this dip for models of the history of the Siletz terrane are discussed in section 5.2.

We assumed that the western edge of the Siletz terrane is a straight line in cross section. However, if one relaxes this condition, many geometries are allowable for the seaward edge of the Siletz terrane below 7-km depth, including a slight landward dip. Figure 6 illustrates the sensitivity of the magnetic model to the thickness of the Siletz terrane and shows that a landward dip at depth shallower than 7-km depth leads

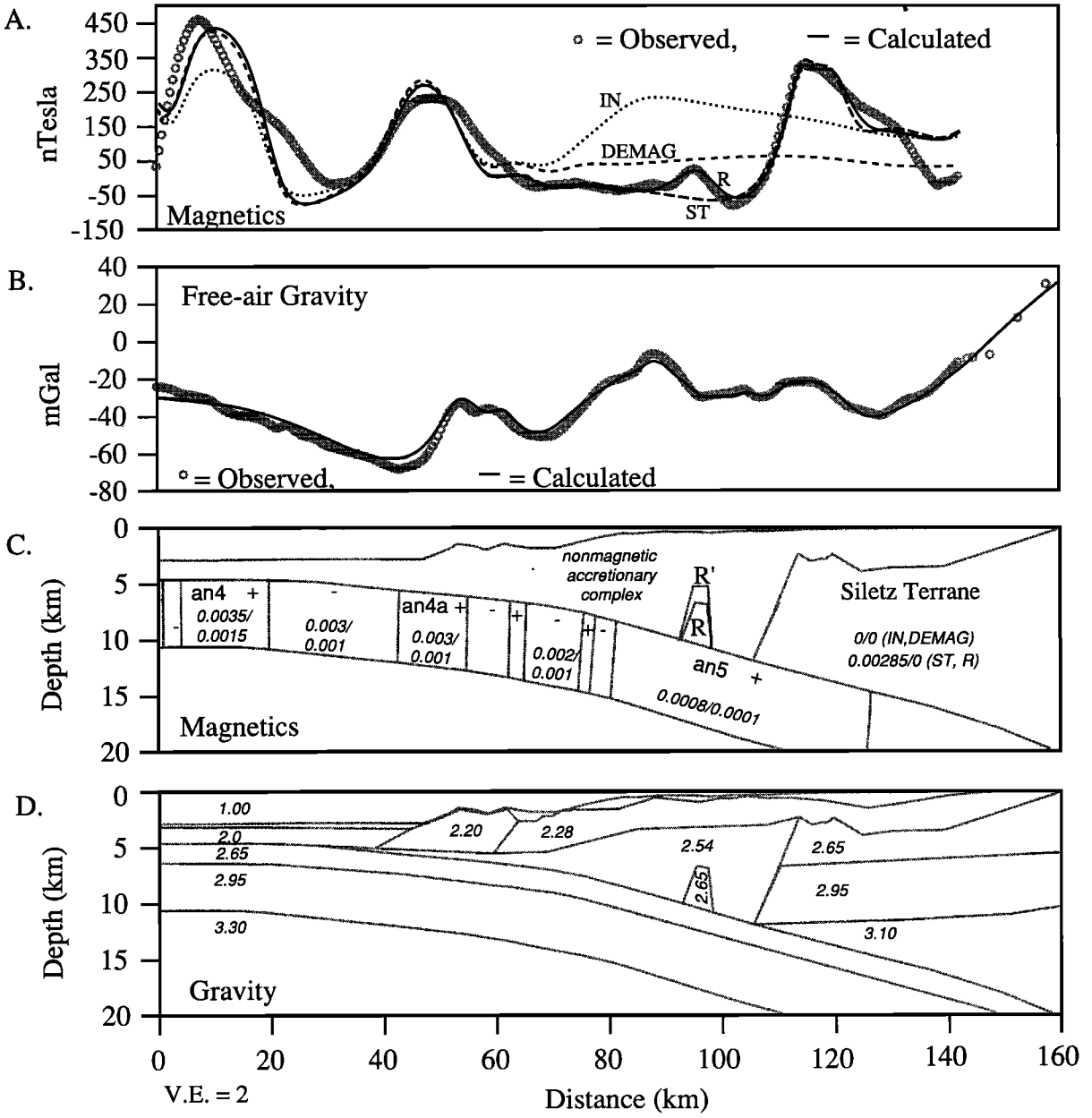

Figure 4. Summary of magnetic and gravity anomaly modeling for the north line. Although the gravity and magnetic anomalies were modeled together using models specified by the same boundaries, as is generally done with crustal potentail field modeling, the results are shown in two separate plots in order to highlight those parts of the model most sensitive to the different data sets. (a) Observed and calculated magnetic anomalies. Steps in the magnetic modeling are described in the text. (b) Observed and calculated gravity anomalies. (c) Magnetic model. Except for the seafloor, which is included for reference, only boundaries of bodies with nonzero magnetic parameters are shown. Magnetic parameters (susceptiblity and remanent magnetization) of the subducted Juan de Fuca plate are shown; "anX" indicates blocks corresponding to identified seafloor spreading anomalies; + and - refer to the sign of the remanent magnetization. Magnetic parameters of the Siletz terrane (ST) and the buried ridge (R and R') are also shown. The strategy for developing the model, which proceeded in steps from initial (IN), to demagnetization of subducted oceanic crust (DEMAG), to buried ridge of oceanic crust (R), to alternate buried ridge model (R'), is discussed in the text. Magnetization properties are in cgs units to be consistent with most prior literature. To convert to SI, multiply susceptibility values by 4π and multiply remanent magnetization values by 10^3 to convert emu/cm^3 to A/m. (d) Gravity model. Only boundaries separating bodies of different density are shown. Densities were determined from the seismic velocity model of *Tréhu et al.* [1994] as described in the text. Densities are in units of 10^{-3} kg/m^3.

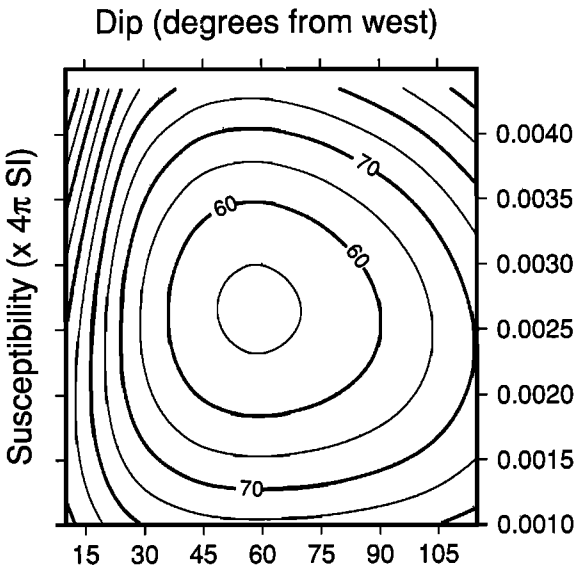

Figure 5. Root-mean-square misfit of the anomaly predicted by the magnetic model as a function of susceptibility and dip of the Siletz terrane. A dip of 90° is vertical; seaward dips are <90°; and landward dips are >90°. The best fitting susceptibility and dip are 0.0025 and 60, respectively.

to a calculated field that does not fit the observed magnetic data, regardless of the susceptibility assumed for the Siletz terrane. The seismic data also require a thick Siletz terrane that extends nearly to the subducting oceanic crust, as shown in Figure 7, which shows ray path coverage and travel time fit for arrivals refracted through the Siletz terrane and underlying oceanic crust and for arrivals reflected from the base of the subducted oceanic crust for the model of *Tréhu et al.* [1994]. These arrivals were recorded on stations deployed onshore to record offshore shots, which provided the best experimental geometry to image the structure beneath the coastline and continental shelf.

The fit of our calculated magnetic anomaly to the observed data is poor around model km 140 (Figure 4a). This is probably due to the Miocene sills mentioned above. The reflection data indicate that these basalts do not extend farther east than model km 130 (Figure 3). We did not include these sills, which require a fully three-dimensional modeling approach, because of their lack of influence on models of the Siletz terrane edge. They could account for the high-amplitude, relatively short-wavelength mismatch here if they have a significant and predominantly reversed remanent magnetization. The limited regional extent of this magnetic low (Figure 2b) supports this interpretation.

The final feature of the magnetic data that we modeled is the local high at km 80-100. This anomaly appears to be part of a low-amplitude, linear, margin-parallel anomaly that begins near 45°00'N and continues to the south to about 43°00'N. This magnetic anomaly was not recognized prior to our study. It is a subtle feature that is not visible in maps scaled to span the range of magnetic anomaly values characteristic of seafloor spreading and the Siletz terrane. However, it is apparent in ship track magnetic data north of Heceta Bank. The expression of this feature can also be enhanced, as shown in Figure 8, by applying a shaded-relief filter and by selecting a finer contour interval. In line with this feature to the south (~42°00'N to ~43°00'N) are several circular positive and negative anomalies that may be buried seamounts offshore Cape Blanco (T. Brocher, personal communication, 1996). The velocity model shows a basement high with velocities appropriate for upper oceanic crust in this region (Figure 1d).

The linear anomaly cannot be modeled as a seafloor magnetic lineament, because its wavelength is too short to be produced by a source at the depth of the subducting crust. The data can, however, be matched by introducing a narrow ridge of material with the same magnetic properties that we assumed in our initial model for positively polarized oceanic crust (K=0.003 and M_R=0.001). The best fitting cross-sectional shape of a body with these magnetic parameters, assuming that it extends to the subducted plate, is shown in Figure 4c (labeled R), and the predicted anomaly is shown by line R in Figure 4a. Assuming that the magnetic parameters that were derived for the Siletz terrane (K=0.00285 and M_R=0) results in a larger, shallower body (labeled R' in Figure 4c) with no perceptible change in the predicted magnetic anomaly. If the magnetic body is smaller and deeper, susceptibility rapidly increases to unrealistic values. It can, however, be somewhat shallower if it is not in contact with the subducting oceanic plate. Several possible interpretations of this feature are discussed in section 5.3.

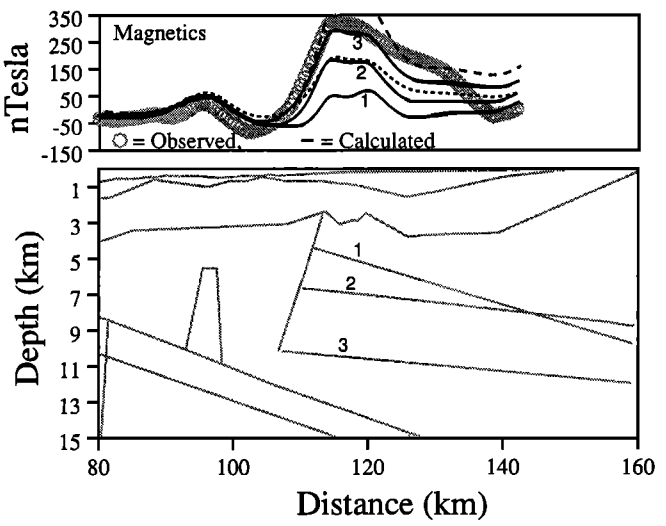

Figure 6. Example of magnetic models showing the sensitivity of the model to variations in the thickness and dip of the seaward part of the Siletz terrane. Lines 1-3 show the effects of varying the configuration of the Siletz terrane while keeping the susceptibility fixed at 0.00285. The dashed lines correspond to model 3 with susceptibility varied by +- 0.0005. Magnetic parameters of the subducted Juan de Fuca plate crust and buried ridge are the same as those in the final model of Figure 4. Magnetic parameters of the accretionary complex, including that portion underlying the Siletz terrane, are 0. A landward dip of the boundary of the base of the Siletz terrane (model 1) moves the main peak of the anomaly to the east. Because the observed peak is fixed, such a model requires that the Siletz terrane extend farther west than is allowed by the seismic data. Assuming the selected magnetic properties are representative, the Siletz terrane probably extends to a depth of at least 7-9 km, consistent with the seismic and gravity data.

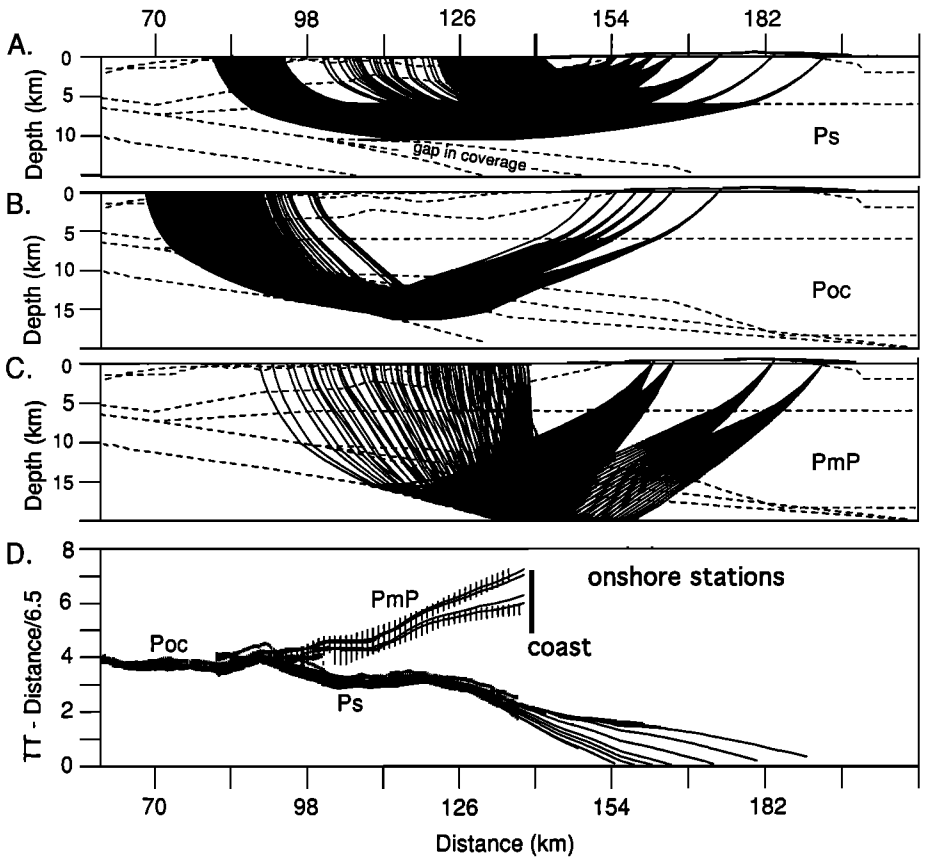

Figure 7. (a-c) Ray diagrams showing coverage of seaward edge of Siletz and underlying Juan de Fuca plate using refracted arrivals turning within the Siletz terrane (*Ps*), refracted arrivals turning within the subducted Juan de Fuca crust (*Poc*), and arrivals reflected from the base of the subducted Juan de Fuca crust (*PmP*). (d) The calculated and observed travel times for all onshore-offshore recordings. The model for the calculations is the same as that shown in Figure 1d and discussed by *Tréhu et al.* [1994, 1995]. A small advance from the buried ridge at km 95 is observed near km 84 in phases labeled *Ps* and *Poc*. The primary evidence for this phase, however, is in the ocean bottom seismometer (OBS) data, which are not discussed in this paper but which show a localized region of oceanic crustal velocities at relatively shallow depth.

3.3. Gravity Model

For the gravity model, subdivision of the accretionary prism and Siletz terrane into several bodies (generally increasing in density arcward and downward) represents, for the most part, the discretization of continuous density gradients implied by the velocity model. Some minor modification of densities from the initial values derived from the velocity model was required to model the gravity data, reflecting uncertainty in the velocity model and in the conversion from seismic velocity to density. The densities in our final gravity model remain consistent with those predicted from the velocity model via the Nafe-Drake relationship (Figure 9), showing that the velocity model of *Tréhu et al.* [1994] is generally consistent with the gravity data. Although we do not show the sensitivity of the model to the thickness of the Siletz terrane and buried ridge since the thickness of the Siletz terrane beneath the shelf has already been demonstrated by the magnetic and seismic modeling, we note that a significant decrease in the thickness or density of the Siletz terrane leads to a poor fit to the data.

The configuration of the subducting plate in this model is significantly different from that in previous crustal models derived from gravity [e.g., *Couch and Riddihough*, 1989], because these previous models were unconstrained by seismic data, and overestimates of the thickness of low-density sediments resulted in an underestimate of the depth to the subducting plate beneath the continental shelf.

4. Modeling: South Line

4.1. Initial Model Parameterization

Our starting model for the profile crossing Heceta Bank was adapted from the cross section of *Snavely et al.* [1985], which is based on seismic reflection lines, regional gravity and magnetics data, an industry well, and onshore surficial geology. This was used to define the shallow basin structure and the distribution of the upper Eocene-age Yachats basalt, which represents basement in the seismic reflection section. This basalt is manifested in the regional magnetics map as a strong, localized high where it outcrops at the coast at ~44°15'N; adjacent, strong, areally limited lows immediately to the north probably represent the same basalt outcrop but reversely magnetized [*Simpson and Cox*, 1977]. The *Snavely et al.* estimate for the geometry of the top of the Siletz terrane was also used in the model. The density structure within the accretionary prism and the configuration of the subducting Juan de Fuca

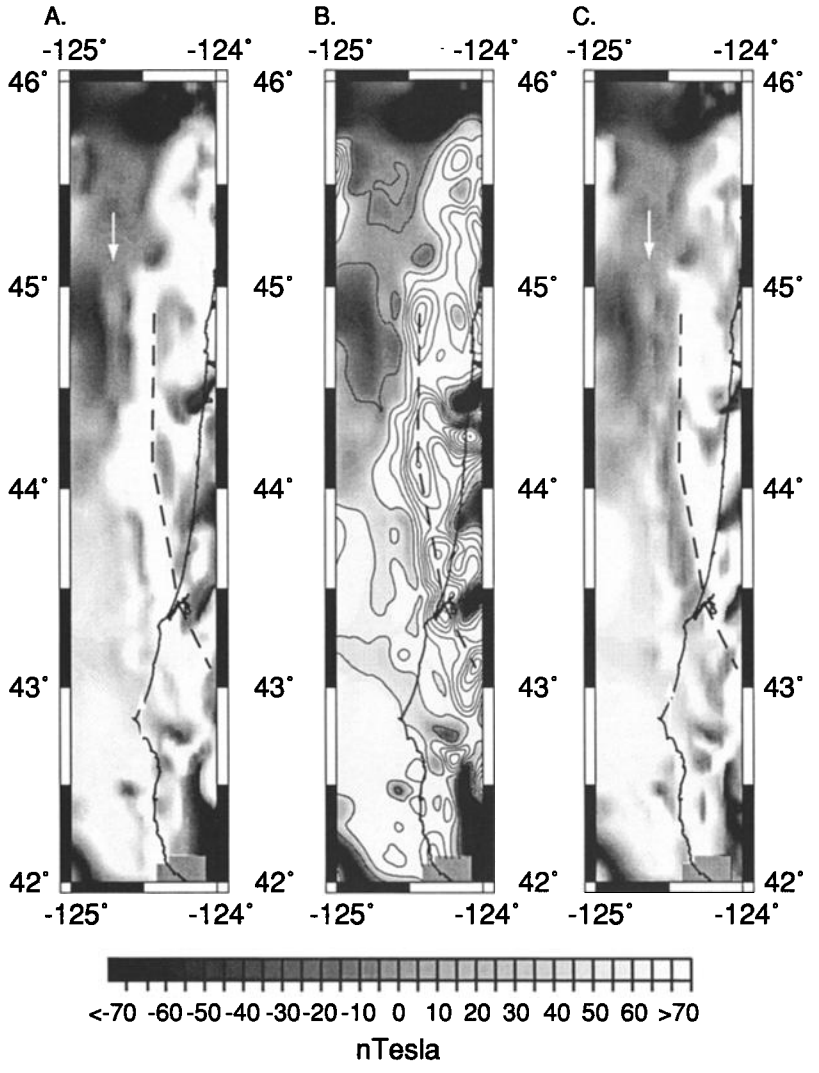

Figure 8. Magnetic anomalies in the region of the seaward edge of the Siletz terrane. Data are the same as those in Figure 2b, but the data are plotted with a palette designed to show low-amplitude anomalies. (a) Illumination from the west. (b) No illumination. Contours at an interval of 60 nT are shown. (c) Illumination from the east. The peak of the anomaly marking the western edge of the Siletz terrane is shown as a dashed line on Figures 8a-8c, and the anomaly due to the buried mafic ridge is indicated by white arrows in Figures 8a and 8c.

plate were taken from our model of the northern line. The regional magnetic anomaly map (Figure 2b) shows that the magnetic lineaments of the Juan de Fuca plate are uninterrupted between the two profiles in this study, supporting the assumption that the subducting plate is continuous between the two profiles.

4.2. Magnetic Model

Initial estimates of K and M_R for the Juan de Fuca plate crust and the Siletz terrane were taken from the modeling results of the north line. Siletz bulk M_R was assumed to be 0 for reasons discussed in section 3.2, and K was assumed to be 0.00285 cgs units. For the Yachats basalt, K and M_R were set to 0.0026 and 0.001 [*Bromery and Snavely*, 1964], and declination and inclination were set to 46° and 64°, respectively [*Simpson and Cox*, 1977]. The response of this initial model is labeled IN in Figure 10a. It includes the eastward demagnetization of the subducted crust determined for the north line and a seaward dip of 57° for the Siletz terrane, as determined for the north line.

In step 2 (labeled CD, for "change dip," on Figure 10a), the susceptibility for the positively magnetized blocks responsible for anomalies 4 and 4a is decreased to 0.002. As for the north line, we do not attempt to interpret this minor change in the magnetic properties of the subducting oceanic crust. In addition, the dip of the western edge of the Siletz terrane was decreased to 30°W, and K is increased to 0.0033. However, it is not clear whether these changes are significant given the uncertainty in the depth and susceptibility of the Siletz terrane.

A small-amplitude, medium-wavelength magnetic anomaly is clearly superimposed on the main Siletz anomaly at model km 102–112 (Figure 10a). This anomaly may be part of the buried "ridge" discussed above for the northern profile, or it may reflect irregularity of the seaward edge of the Siletz ter-

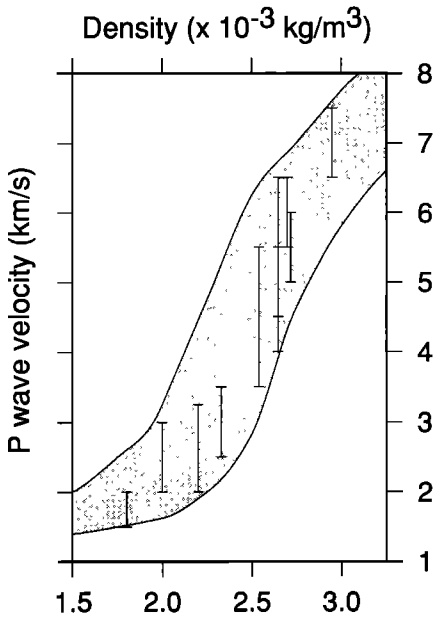

Figure 9. Relationship between density in the final model of Figure 4d and velocity in Figure 1d. The range of velocities for each density results from the different model parameterizations: The velocity model is dominated by gradients whereas the density model is constructed from a small number of isodensity bodies. The shaded region shows the range of experimental data. The final velocity-density relationship is within the allowable range of densities.

rane. These two possibilities are discussed in section 5.3. Assuming K, M_R, D, and I of 0.003, +-0.001, 19°, and 69°, respectively, and finding the cross section of a linear body that fits the magnetic data results in the feature labeled R in Figure 10a and predicted anomaly R in Figure 10a. Assuming magnetic parameters appropriate for the Siletz terrane (K=0.00285 and M_R=0) results in the feature labeled R' in Figure 10c. While there is some trade-off between the magnetic parameters and geometry of this body and while details of the structural relationship between the ridge and the Siletz terrane cannot be resolved, if the anomaly is from a buried ridge, then the ridge is in contact with the Siletz terrane in this region.

4.3. Gravity Model

The primary objective of modeling the gravity anomaly on this profile was to place constraints on the density structure beneath Heceta Bank. Step 1 (Figure 10b) shows the anomaly predicted using the density structure obtained for the northern line, with the density of accretionary complex material increasing landward and with depth in three steps. The dashed line shows the boundary between a density of 2.28 x 10^{-3} kg/m^3 above and 2.54 x 10^{-3} kg/m^3 below in the initial model; the density of the outer part of the accretionary complex is 2.2 x 10^{-3} kg/m^3 in the initial model. The anomaly predicted by this model indicates that the model density is too high beneath the outer accretionary complex and too low beneath Heceta Bank. Lowering the density in the outer accretionary complex from 2.2 to 2.0 x 10^{-3} kg/m^3 and moving the boundary between material with a density of 2.28 x 10^{-3} and 2.54 x 10^{-3} kg/m^3 to near the seafloor beneath Heceta Bank improves the fit of the predicted anomaly to the data (anomaly labeled HB in Figure 10b and shaded region in Figure 10d). Low densities in this region are consistent with the interpretation of *Goldfinger et al.* [1999] that this region is a large slump.

There is a significant trade-off between the density and the shape of the high-density core beneath Heceta Bank. Assuming a density of 2.7 x 10^{-3} kg/m^3 results in lowering the boundary between the upper and lower accretionary complex by ~2 km. A body with this density would most likely be made of basalt and would probably represent a subducted seamount. Although we cannot rule out a concealed seamount, with magnetic properties such that the effects of induced and remanent magnetization cancel each other such that no magnetic anomaly is produced, we consider this interpretation highly unlikely. Our gravity model therefore suggests that high-density middle Miocene and older sediments of the deep accretionary complex have been uplifted to form the core of Heceta Bank, as originally suggested by *Kulm and Fowler* [1974], and places limits on the volume of material uplifted.

5. Discussion

5.1. Demagnetization of Juan de Fuca Plate Crust

As shown in section 4.3, modeling the seafloor spreading anomalies over the Juan de Fuca plate suggests that the subducted crust is significantly demagnetized. Although the Cascadia subduction zone is characterized by high heat flow due to the young age of the Juan de Fuca plate and the insulating effects of thick sediment cover, thermal models of Cascadia [*Hyndman and Wang*, 1993; *Oleskevich*, 1994] suggest that Curie temperatures of 550°-600°C are not reached on the thrust plane until ~175-200 km east of the deformation front. It is therefore difficult to attribute the observed demagnetization entirely to thermal demagnetization of the subducted plate, assuming a reasonable thermal gradient in the oceanic crust beneath the thrust zone.

We suggest that hydrothermal alteration of the subducted crust also contributes to reducing the remanent magnetization of the subducted crust through metamorphism of the basalt and recrystallization of iron-titanium oxides [*Scheidegger*, 1984; *Finn*, 1990]. Large volumes of fluids released at greater depth by prograde metamorphism of hydrated basalt [*Peacock*, 1987] may be channeled trenchward along the shear zone and may contribute to additional hydrothermal alteration and demagnetization of the subducted crust. Stable oxygen isotopic analysis of carbonate cements in accreted sediments at the central Oregon deformation front indicates circulation of high-temperature fluids upward from the decollement [*Sample et al.*, 1993]. The petrogenetic grid compiled by *Cloos* [1993] suggests that for a young subduction zone, significant metamorphism may take place in the subducting plate at the depths where we require demagnetization. The presence of turbidite-hosted mesothermal gold deposits within the Alaskan accretionary prism also supports the circulation of hot fluids through the forearc [*Hauessler et al.*, 1995].

5.2. Dip of the Western Boundary of Siletz

The geologic history of the western boundary of the Siletz terrane is enigmatic. *Snavely et al.* [1980], on the basis of qualitative evaluation of the potential field data and offshore drill holes, postulated that the western boundary of the Siletz terrane is an Eocene age strike-slip fault that has had at least 200 km of offset and that juxtaposes accretionary melange

against the Siletz terrane. They called this structure the Fulmar fault, and they called the outboard terrane the Fulmar terrane. Onlap by late Eocene sediments on the continental shelf near 43°N suggests that motion on the Fulmar fault was essentially complete by 43 Ma. The Fulmar fault may thus have been part of a larger right-lateral fault system that dispersed terranes such as the Yakatat terrane along the margin of North America [*Snavely and Wells*, 1996]. The steep seaward dip of the western edge of the Siletz terrane in our potential-field models supports the concept that the western edge of the

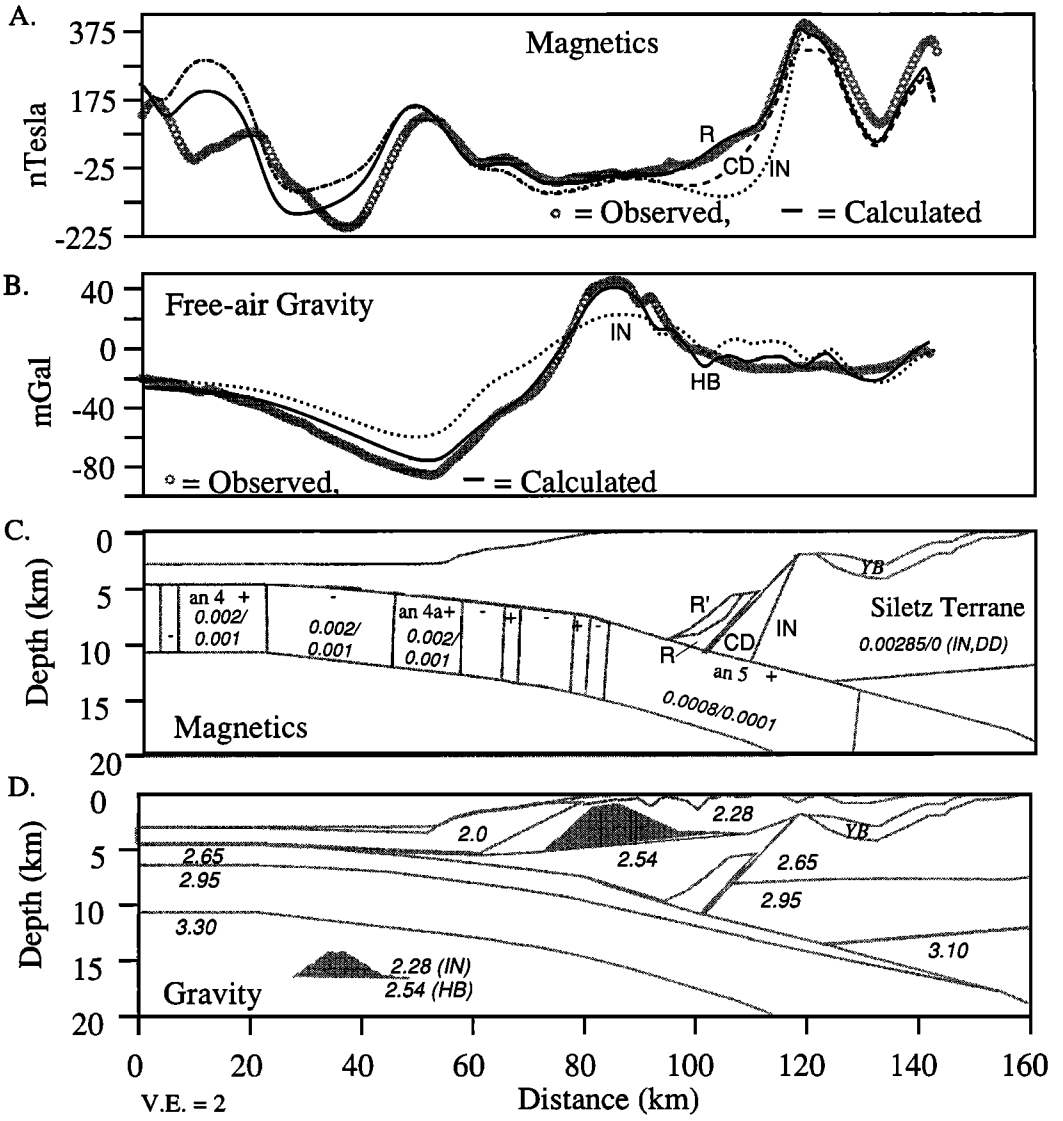

Figure 10. Summary of magnetic and gravity anomaly modeling for the south line. Steps in the modeling are discussed in the text. Gravity and magnetic modeling results are shown in different for reasons discussed in Figure 4. (a) Observed and calculated magnetic anomalies. (b) Observed and calculated gravity anomalies. (c) Magnetic model. Except for the seafloor, which is included for reference, only boundaries of bodies with nonzero magnetic parameters are shown. The model was developed by modifying an initial model (IN) derived from the northern profile. The magnetic model was modified by changing the dip of the Siletz terrane (CD), followed by adding a buried ridge of oceanic crust (R) or Siletz terrane (R'). The gravity model was changed by increasing the density beneath Heceta Bank (HB) and decreasing the density to the west. Magnetic parameters (susceptibility and remanent magnetization) of the Siletz terrane and of the subducted Juan de Fuca plate are shown ("anX" indicates blocks corresponding to identified seafloor spreading anomalies; + and - refer to the sign of the remanent magnetization). Magnetization properties are given in cgs units to be consistent with most prior literature. To convert to SI, multiply susceptibility values by 4π multiply remanent magnetization values by 10^3 to convert emu/cm^3 to A/m. (d) Gravity model. Only boundaries separating bodies of different density are shown. Densities were determined from the seismic velocity model of *Tréhu et al.* [1994] as described in the text and are in units of 10^{-3} kg/m^3. Modification of the initial density distribution is shown as the shaded region, which shows uplift of material with densities appropriate for deeply buried accretionary complex sediments. Densities seaward of this region are lower than those assumed for the initial model, supporting the suggestion of *Goldfinger et al.* [1999] that this material represents a recent slump.

Siletz terrane in this region was truncated by strike-slip faulting. One would expect that an intact relict subduction boundary would dip landward, as has been suggested for the western boundary of the Siletz terrane beneath Washington [*Finn*, 1990; *Aprea et al.*, 1998]. The extensional faulting recorded by the Siletz basement topography on the north line (Figure 3) may also be a relict of this tectonic episode, resulting from an extensional offset in the Fulmar fault.

5.3. The Buried Mafic Ridge

Several geologic interpretations are possible for the buried basaltic ridge that we have identified and modeled on the basis of detailed examination of the magnetic field. We rule out an origin as typical abyssal hill topography, because such features are an order of magnitude smaller [*Macdonald et al.*, 1996].

One possibility (model A) is that the ridge represents a sliver of Siletz terrane crust that was sheared off from the main part of the terrane by a right-lateral strike-slip fault that was oblique to the seaward edge of the Siletz terrane. Similar but smaller slivers of crust have been mapped along the boundary between Crescent terrane and accretionary complex material on the Olympic peninsula [*Tabor et al.*, 1972]. It is, however, difficult to reconstruct a kinematic history that explains why the ridge should be in contact with the Siletz terrane beneath Heceta Bank but separate from it both to the north and south of the bank. Assuming that the strike-slip activity responsible for this terrane distribution occurred during the Eocene, this model also implies that separation between the Siletz sliver and the main Siletz terrane has been preserved through nearly 50 million years of compressional tectonics, which we consider unlikely.

A second possibility (model B) is a ridge of upper oceanic crust that is forming in place by imbrication and thickening of the subducted oceanic crust in response to compression. Such features have been inferred to exist in the relict subduction zone of the central California continental margin [*Miller and Howie*, 1993]. This model implies that the plate boundary has stepped down into the crystalline crust of the Juan de Fuca plate, transferring material from the lower plate to the upper plate. We expect that the thrust fault at the core of such a ridge forming in oceanic crust at these depths would be marked by seismicity, which is not observed.

A third possibility (model C) is that the ridge represents a subducted aseismic ridge or seamount chain formed by constructional volcanism in the ocean basin along a line parallel to the spreading center. In this model, the ridge has been dragged obliquely through the accretionary complex for the past 1.2 million years (Figure 11). Several examples of subducted ridges or seamounts have been identified in other subduction zones and have been shown to have a considerable effect on the development of the accretionary complex along the path of the subducted seamount [e.g., *Lallemand and Le Pichon*, 1987; *von Huene and Scholl*, 1991; *von Huene et al.*, 1996]. Because the inferred ridge is approximately parallel to magnetic lineations, it probably was not formed at a leaky transform fault. Moreover, because the ridge does not appear to be offset where it intersects the landward projection of a pseudofault generated by a propagating rift [*Wilson*, 1993], it could not have formed at a spreading ridge. Few, if any, analogous seafloor ridges (parallel to the spreading center but formed off axis) are observed in the present ocean basins. We note, however, that such a ridge could have formed beneath the accretionary complex farther west and then have been transported to its present position, combining models B and C.

A variation of this model (model C') is that the ridge was formed from seamounts that have been partially subducted and then transferred from the Juan de Fuca to the North American plate. In this model, the thick Siletz terrane may prevent subduction of seamounts. The ridge may thus represent the "flotsam and jetsom" of subduction, accumulated over several million years. This model, however, does not explain why the ridge appears to be in contact with the Siletz terrane only beneath Heceta Bank, unless the position where seamounts are sheared off the lower plate is not directly determined by the position of the Siletz backstop (see section 5.5).

5.4. Possible Impact on History and Morphology of the Accretionary Complex

Each of these models predicts a different pattern of uplift and subsidence of the overlying accretionary complex. Model A predicts no post-Eocene uplift or subsidence directly related to the ridge, although other processes active along the margin (e.g., rotation of the ridge relative to the main Siletz backstop) might have caused uplift or subsidence during this time period. Model B predicts a stationary center of uplift overlying the ridge as it forms but no pronounced subsidence. Models C and C' predict the greatest uplift and subsidence, with the margin being first uplifted as the ridge passes through and then subsiding in its wake [*von Huene and Scholl*, 1991]. Timing of uplift and subsidence, however, is different for the two models. Model C predicts uplift and subsidence only during the past 1.2 m.y.b.p., with uplift and subsidence being nearly simultaneous along 200 km, whereas model C' predicts a longer, complex history of localized uplift and subsidence.

Considerable Miocene and later uplift and subsidence are recorded in the morphology and stratigraphy of the continental margin [e.g., *Snavely*, 1987; *Snavely and Wells*, 1996; *Yeats et al.*, 1998] as indicated by "textbook" examples of unconformities in the marginal basin stratigraphy (Figure 3). Regional mapping of the Miocene-Pliocene unconformity [*McNeill et al.*, 1998] shows that the late Miocene outer arc high continues north of Heceta Bank beneath what is now the continental slope to at least 46°N, where it lies beneath the outer edge of Nehalem Bank. Nehalem Bank is similar in size to Heceta Bank but is not associated with either a magnetic or a gravity high [*Fleming*, 1996], suggesting a different origin (Figure 2). Because portions of the outer arc high are now beneath the continental slope, *McNeill et al.* (1998) proposed later slope instability or subsidence due to subduction erosion. This period of forearc evolution may predate formation of the buried ridge since the late Miocene forearc high extends north of where the buried ridge is observed.

More recently, three massive landslides have been documented along the Cascadia margin west and southwest of Heceta Bank by *Goldfinger et al.* [1999], who conclude that subducted seamounts may have triggered the slides by basal erosion of the accretionary complex as they passed beneath it. The locations of the slides are shown in Figure 11 and compared to the current position of the buried ridge and its track for the last 2 million years, as predicted by the Juan de Fuca-North America plate vector [*DeMets et al.*, 1990] assuming

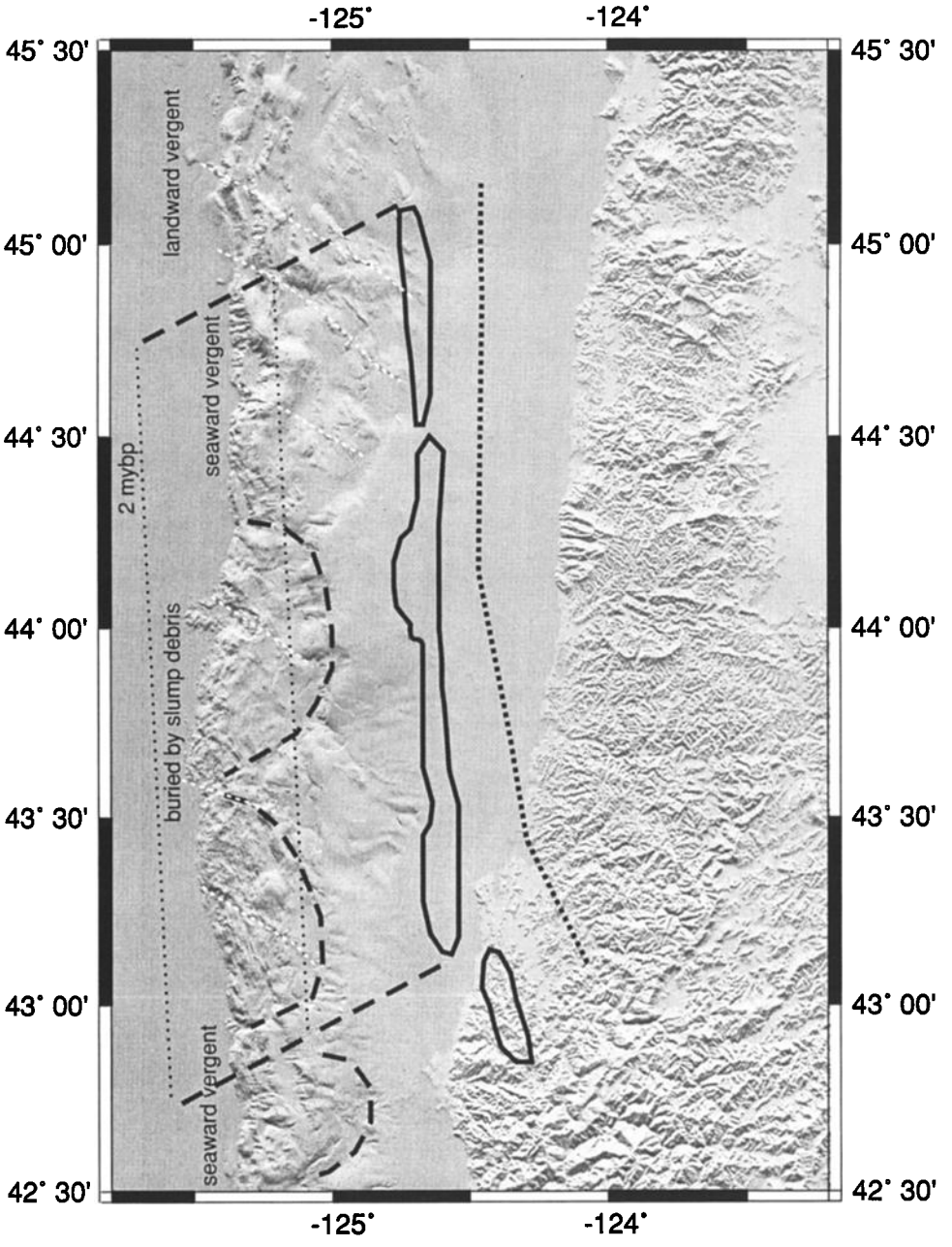

Figure 11. Morphology of the Oregon continental margin, shown as a shaded surface illuminated from the north. Topographic data from multiple onshore and offshore data sets were compiled and regridded by C. Goldfinger. Overlain on this surface are the location of the seaward edge of the Siletz terrane (heavy dotted line), the buried mafic ridge as inferred from the magnetic anomalies (heavy solid line), the headwalls of major Neogene slumps (dashed lines); [from *Goldfinger et al.*, 1999], and the position of left-lateral strike-slip faults that cut the accretionary complex (white dashed lines) [from *Goldfinger et al.*, 1997]. The predicted track of the buried ridge through the accretionary complex assuming the NUVEL plate motion vector [*DeMets et al.*, 1990] is shown by the diagonal heavy dashed lines, and the predicted location of the ridge 1 and 2 million years ago, assuming model C, is shown by the light dotted lines. For model C any seamounts contributing to the buried ridge must have been east of these lines 1 and 2 million years ago.

model C. A similar track would be followed by any seamounts subducted with the Juan de Fuca plate within the past 8 million years, the time of the most recent major changes in relative motions of the Pacific and Juan de Fuca plates [*Wilson*, 1993] and the Pacific and North American plates [*Atwater and Stock*, 1998]. However, the buried ridge extends well north of the megaslumps. Inferred ages of the megaslumps, which are 110, 450, and 1120 kyr, increasing from north to south, are also generally incompatible with subduction of an aseismic ridge or a series of seamounts. It may, however, have led to conditions favorable for slumping along this part of the margin by inhibiting subduction, leading to thickening and oversteepening of the accretionary complex and triggering of slides in response to earthquakes with hypocenters farther east.

The northern boundary of the predicted track of the subducted ridge does correlate with a major change in slope morphology and deformation front structure. North of the buried

ridge, the margin is marked by a series of ridges formed by distributed landward vergent thrusting [*Flueh et al.*, 1998]. Where the subducted ridge and seamounts are predicted to have passed, the slope morphology is more irregular, and the deformation front is generally characterized by a seaward vergent thrust [*MacKay*, 1995]. Vergence direction is obscured by slump debris from 43°N and 44°N, but a seaward vergent basal thrust is observed cutting through older slump debris between 42°N to 43°N [*Goldfinger et al.*, 1999]. South of 42°N, where the Siletz terrane is absent and the crystalline backstop of the Klamath terrane forms a landward dipping backstop [*Beaudoin et al.*, 1996], vergence appears to be mixed [*Gulick et al.*, 1998]. These changes in vergence at the deformation front have been previously attributed to differences in pore pressure on the decollement resulting from differences in the thickness and composition of sediments on the subducting plate. While we find this interpretation well justified, the correlation with the massive Siletz backstop and buried mafic ridge suggests a feedback effect in which the along-strike variation in sediment properties on the subducting plate is due, in part, to differences in the uplift and subsidence history of the adjacent accretionary complex.

The buried ridge also correlates well with the portion of the margin characterized by northwest trending strike-slip faults (Figure 1) [*Goldfinger et al.*, 1997, 1999]. While a few strike-slip faults have been mapped farther north, only along this portion of the margin are they well defined and regularly spaced. None of these faults extend east of the seaward edge of the Siletz terrane, and they rapidly die out in the abyssal plain. These faults imply N-S extension of the sliver of accretionary complex caught between the deformation front and Siletz terrane.

Although we cannot definitively rule out any of the four possible explanations for the buried mafic ridge and none of the models is consistent with all of the available geologic data, the apparent correlation between the predicted track of a subducted ridge through the accretionary complex, variations in slope morphology and deformation front structure, and the left-lateral strike-slip faults cutting the accretionary complex lead us to favor model C'. We suggest that subducted seamounts rafted in on the subducting plate over roughly the past 8 million years have accumulated through time to form an apparent buried ridge. The presence of this ridge may further inhibit subduction of accretionary complex material, leading to east-west shortening and north-south extension, uplift of lower accretionary complex material, oversteepening of slopes, and massive slope collapse.

5.5. Subduction Zone Asperities

Regardless of the optimum model for formation of the ridge, it likely results in a change in the material properties across the plate boundary [*Dmowska et al.*, 1996] and thus may represent an asperity, or region of higher frictional resistance, along the plate boundary. If this is the case, then the lack of seismicity in this region may be due to plate locking. Geodetic evidence for plate locking is ambiguous. This region is a node in both long-term and short-term measurements of uplift [Mitchell et al., 1994], leading to the hypothesis that the plate boundary is not locked in this region. However, recent Global Positioning System (GPS) measurements indicate horizontal motions in the Coast Range and Willamette Valley indicative of locking [*McCaffrey et al.*, 1998]. Within the next few years, ongoing geodetic work should provide new information about current plate interactions. The crustal parameters determined by this study and other studies will provide important constraints on geodynamic models to explain the observed geodetic data.

In the case of models B and C, we must further consider the effect of topography on the plate interface as it must pass over the top of the buried ridge. *Cloos* [1992, 1993] has argued that large seamounts will be too buoyant to be subducted, locking the subduction zone until the stress increases enough to shear them off and transfer them to the upper plate. *Scholtz and Small* [1997] consider a more general case of the effect of a subducting seamount that includes the effects of flexure. While they conclude that seamounts will not always be transferred to the upper plate, their model predicts that a 4-km-high seamount will contribute significantly to the normal stress and that the effect of subducting seamounts is especially pronounced in generally decoupled subduction zone. Either model predicts temporary locking and eventual stress release in large earthquakes.

Offshore Oregon, the buried ridge may have been subducted to a depth at which the frictional resistance to subduction on the plate boundary exceeded the stress required to shear off the subducting seamount. The influence of the Siletz backstop on this process, which depends on the slope and height of the subducted seamount and on the flexural strength of the upper and lower plates, is uncertain. If thickening and dewatering of the accretionary complex alone are adequate to increase the normal stress on the plate boundary enough for the plate boundary to jump to the base of a seamount, then model C' is compatible with the observation that the buried ridge is not in contact with the Siletz terrane along much of its length. However, if this is the case, the correlation between the buried ridge and the Siletz terrane may be coincidental. Geodynamic models of stresses resulting from interaction between the Siletz backstop and buried ridge are needed to resolve this question. Regardless of whether the seaward dipping western edge of the Siletz is causing seamounts to be sheared off the subducting plate, the process of breaking through oceanic crust on this scale is likely to be seismogenic. *Scholtz and Small* (1997) note that large earthquakes seem to have resulted from this process in the normally decoupled Tonga-Kermadec and Izu-Bonin arcs.

6. Conclusions

Magnetic and gravity modeling in conjunction with existing geologic and geophysical constraints indicates that the western edge of the Siletz terrane, which acts as the subduction zone backstop, has a seaward dip of less than 60° (measured from horizontal). The Siletz terrane may continue to descend at these dips to the subducting Juan de Fuca plate, but alternative geometries for the lowermost portion of the backstop are also consistent with the potential-field data. Underthrusting of more than ~2 km of accretionary complex material, however, is unlikely. This steep, seaward dip supports the *Snavely et al.* [1980] model for Eocene strike-slip truncation of the Siletz terrane, rather than maintenance of an undeformed relict subduction boundary since accretion of the Siletz terrane. The magnetic data also require progressive eastward demagnetization of the Juan de Fuca crust in the magnetic quiet zone, which is most likely due to a combination of thermal and chemical demagnetization. Our southern transect reveals that Heceta Bank is cored by relatively dense sediments (~2.54 g/cm^3), which likely represent uplift, older, denser, sedimen-

tary rocks that were previously deeply buried within the accretionary complex.

Perhaps the most important result of our investigation is the identification of a mafic ridge buried beneath the accretionary complex from about 45°N to 43°N. From correlation between the location of the buried ridge, seafloor morphology, and the recent geologic history of the margin, we conclude that the ridge represents seamounts rafted in over the past several million years. We propose that subduction of these seamounts is impeded by the thick, seaward dipping Siletz backstop, leading to a complicated feedback between accretionary complex uplift, subsidence, collapse, and faulting. Other possible origins include formation in place through imbrication of the subducting crust and formation as a sliver of Siletz during the Eocene period of strike-slip tectonics that formed the seaward dipping backstop. Regardless of its origin, the ridge likely represents a contrast in the physical properties of the plate boundary and may therefore be acting as an asperity on the megathrust, although the details of this process are ambiguous.

The seaward dipping backstop formed by the thick Siletz basalts that we model for the central Oregon margin contrasts with the landward dipping backstop formed by this terrane beneath Washington [e.g., *Finn*, 1990; *Aprea et al.*, 1998] and by the Klamath terrane beneath northern California [*Tréhu et al.*, 1995; *Beaudoin et al.*, 1996]. These different backstop geometries may be, in part, responsible for the different patterns of deformation observed in the accretionary complex of Oregon and Washington.

Acknowledgments. We thank Northwest Geophysical Associates (Corvallis, OR) for use of their potential-field modeling software. Vern Kulm and Bob Yeats provided many helpful comments over the course of this work. Lisa McNeill, Tom Hildebrand, Carol Finn, and Ray Wells provided careful reviews. Christof Lendl provided technical assistance with data processing and display. The location map in Figure 1a was modified from a figure prepared by Ray Wells. Many of the figures in this paper were created using Generic Mapping Tools [*Wessel and Smith*, 1991]. Research was supported by the U.S. Geological Survey (USGS), Department of the Interior, under USGS award 1434-95-G-2617 to Oregon State University. The views and conclusions contained in this document are those of the authors and should not be interpreted as necessarily representing the official policies, either expressed or implied, of the U.S. Government.

References

Aprea, C., M. Unsworth, and J. Booker, Resistivity structure of the Olympic mountains and Puget lowland, *Geophys. Res. Lett.*, *25*, 109-112, 1998

Atwater, T., and J. Stock, Implications of recent refinements in Pacific-North America plate tectonic reconstructions, *Eos Trans. AGU*, *79*(45), Fall Meet. Suppl., F206, 1998.

Beaudoin, B.C., et al., Transition from slab to slabless: Results from the 1993 Mendocino triple junction seismic experiment, *Geology*, *24*, 195-199, 1996.

Bromery, R.W., and P.D Snavely Jr , Geologic interpretation of reconnaissance gravity and aeromagnetic surveys in northwestern Oregon, *U.S. Geol. Surv. Bull 1181-N*, 1964.

Butler, R.F., *Paleomagnetism: Magnetic Domains to Geologic Terranes*, 319 pp., Blackwell Sci., Cambridge, Mass., 1992

Byrne, D.E , W. Wang, and D.M Davis, Mechanical role of backstops in the growth of forearcs, *Tectonics*, *12*, 123-144, 1993.

Cande, S.C., and D.V. Kent, A new geomagnetic polarity time scale for the late Cretaceous and Cenozoic, *J. Geophys. Res.*, *97*, 13,917-13,951, 1992.

Cloos, M , Thrust-type subduction-zone earthquakes and seamount asperities: A physical model for seismic rupture, *Geology*, *20*, 601-604, 1992.

Cloos, M., Lithospheric buoyancy and collisional orogenesis: Subduction of oceanic plateaus, continental margins, island arcs, spreading ridges, and seamounts, *Geol. Soc. Am. Bull.*, *105*, 715-737, 1993.

Coffin, M.F., and O. Eldholm, Scratching the surface: Estimating dimensions of large igneous provinces, *Geology*, *21*, 515-518, 1993.

Couch, R.W., and R P Riddihough, The crustal structure of the western continental margin of North America, in *Geophysical Framework of the Continental United States*, edited by L.C. Pakiser and W.D. Mooney, *Mem. Geol. Soc. Am.*, *172*, 103-128, 1989.

Cranswick, D.J., and K A. Piper, Geologic framework of the Washington-Oregon continental shelf: Preliminary findings, *U.S Geol. Surv. Circ. 1092*, 146-151, 1991.

Davis, D.M., J. Suppe, and F.A. Dahlen, Mechanics of fold-and-thrust belts and accretionary wedges, *J Geophys. Res*, *88*, 1153-1172, 1983.

DeMets, C , R G Gordon, D.F. Argus, and S. Stein, Current plate motions, *Geophys. J. Int.*, *101*, 423-478, 1990.

Dmowska, R., G. Zheng, and J.R. Rice, Seismicity and deformation at convergent margins due to heterogeneous coupling, *J. Geophys. Res.*, *101*, 3015-3029, 1996.

Duncan, R.A., A captured island chain in the Coast Range of Oregon and Washington, *J. Geophys Res.*, *87*, 10,827-10,837, 1982.

Finn, C., Geophysical constraints on Washington convergent margin structure, *J. Geophys. Res.*, *95*, 19,533-19,546, 1990.

Fleming, S.W., Bulldozer blades and colliding submarine mountain chains: Constraints on central Oregon convergent margin tectonics from magnetics and gravity, M.S. thesis, 84 pp., Oreg. State Univ., Corvallis, 1996.

Flueh, E.R., M.A. Fisher, J. Bialas, J.R. Childs, D. Klaeschen, N. Kukowski, T. Parsons, D.W. Scholl, U. ten Brink, A.M. Tréhu, and N. Vidal, New seismic images of the Cascadia subduction zone from cruise SO108 – Orwell, *Tectonophysics*, *293*, 69-84, 1998.

Geophysics of North America [CD-ROM set, version 1.0], http://www.ngdc.noaa.gov, *National Geophysical Data Center*, Boulder, CO, 1987.

Godfrey, N.J., B.C. Beaudoin, S.L. Klemperer, and MTJSE Working Group, Ophiolitic Basement to the Great Valley forearc basin, California, from seismic and gravity data: Implications for crustal growth at the North American continental margin, *Geol. Soc. Am. Bull.*, *108*, 1536-1562, 1997.

Godson, R.H., Description of magnetic tape containing conterminous U S. magnetic data in a gridded format, *U.S. Geol. Surv. Open File Rep., PB87-126017/XAB*, 1987.

Godson, R.H., and D.M. Scheibe, Description of magnetic tape containing conterminous U.S. gravity data in gridded format, *U S. Geol. Surv. Open File Rep. PB82-254798*, 1982.

Goldfinger, C., L.D. Kulm, R.S. Yeats, B. Appelgate, M.E. MacKay, and G F. Moore, Transverse structural trends along the Oregon convergent margin: Implications for Cascadia earthquake potential and crustal rotations, *Geology*, 20, 141-144, 1992.

Goldfinger, C., L.D. Kulm, R.S. Yeats, L. McNeill, and C. Hummon, Oblique strike-slip faulting of the central Cascadia submarine forearc, *J. Geophys. Res.*, *102*, 8217-8243, 1997.

Goldfinger, C , L D. Kulm, L.C. McNeill, and P. Watts, Super-scale failure of the southern Oregon Cascadia margin, *Pure Appl. Geophys.*, in press, 1999.

Gulick, S.P.S., A. M. Meltzer, and S.H. Clarke Jr., Seismic structure of the southern Cascadia subduction zone and accretionary prism north of the Mendocino triple junction, *J. Geophys. Res.*, *103*, 27,207-27,222, 1998.

Hauessler, P.J., D. Bradley, R. Goldfard, L. Snee, and C. Taylor, Link between ridge subduction and gold mineralization in southern Alaska, *Geology*, *23*, 995-998, 1995.

Hussong, D.M., L.K. Wipperman, and L.W. Kroenke, The crustal structure of the Ontong Java and Manihiki oceanic plateaus, *J. Geophys. Res.*, *84*, 6003-6010, 1979.

Hyndman, R.D., The lithoprobe corridor across the Vancouver Island continental margin. The structural and tectonics consequences of subduction, *Can. J. Earth Sci.*, *32*, 1777-1802, 1995.

Hyndman, R.D., and K. Wang, Thermal constraints on the zone of major thrust earthquake failure: The Cascadia subduction zone, *J. Geophys. Res.*, *98*, 2039-2060, 1993.

Kulm, L.D., and G.A. Fowler, Oregon continental margin structure and stratigraphy. A test of the imbricate thrust model, in *The Geology of Continental Margins*, edited by C.A. Burke and C.L. Drake, pp. 261-283, Springer-Verlag, New York, 1974

Lallemand, S, and X Le Pichon, Coulomb wedge model applied to the subduction of seamounts in the Japan trench, *Geology, 15*, 1065-1069, 1987.

Ludwin, R.S., C.S. Weaver, and R S. Crosson, Seismicity of Oregon and Washington, edited by D.B. Slemmons et al., in *Decade Map*, vol. 1, *Neotectonics of North America*, pp. 77-98, Geol. Soc. of Am., Boulder, Colo., 1991.

MacDonald, K.C., P.J. Fox, R.T. Alexander, R. Pockalny, and P. Gente, Volcanic growth faults and the origin of Pacific abyssal hills, *Nature, 380*, 125-129, 1996.

MacKay, M.E., Structural variation and landward vergence at the toe of the Oregon accretionary prism, *Tectonics, 14*, 1309-1320, 1995.

Marine Trackline Geophysics [CD-ROM set, version 3 2], http://www.ngdc.noaa.gov, *National Geophysical Data Center*, Boulder, CO, 1996.

McCaffrey, R., C. Goldfinger, M.H. Murray, P. Zwick, J.L. Nabelek, and C.K. Johnson, GPS constraints on forearc sliver motion, plate coupling, and strain partitioning in northwestern Oregon (abstract), *Eos Trans. AGU, 79*(45), Fall Meet. Suppl., F875, 1998.

McNeill, L.C., L.D. Kulm, C. Goldfinger, and R.S. Yeats, Evolution of the late Neogene central Cascadia forearc basin: investigations of a late Miocene unconformity, Ph.D. thesis, Oreg. State Univ., Corvallis, 1998.

Miller, K.C., and J. Howie, Integrated crustal structure across the south central California margin: Santa Lucia Escarpment to San Andreas fault, *J. Geophys. Res., 98*, 8173-8196, 1993.

Mitchell, C.E., P. Vincent, R.J. Weldon II, and M.A. Richards, Present-day vertical deformation of the Cascadia margin, Pacific Northwest, USA, *J. Geophys. Res., 99*, 12,257-12,277, 1994.

Nelson, A.R., et al., Radiocarbon evidence for extensive plate-boundary rupture about 300 years ago at the Cascadia subduction zone, *Nature*, 378, 371-374, 1995.

Oleskevich, D.A., Comparison of thermal constraint modelling on selected profiles along the Cascadia subduction zone, Work team report, Univ. of Victoria Sch. of Earth and Ocean Sci., Victoria, B.C., Canada, 1994.

Parsons, T, et al., A new view into the Cascadia subduction zone and volcanic arc: Implications for earthquake hazards along the Washington margin, *Geology*, 26, 199-202, 1998.

Peacock, S.M, Thermal effects of metamorphic fluids in subduction zones, *Geology, 15*, 1057-1060, 1987.

Peterson, C.P., P.W. Loubere, L.D. Lulm, and J.S. Peper, Stratigraphy of continental shelf and coastal region, in *Western North American Continental Margin and Adjacent Ocean Floor off Oregon and Washington, Ocean Margin Drill. Prog. Reg. Atlas Ser.*, atlas 1, edited by L.D. Kulm, sheet 8, Mar. Sci. Int., Woods Hole, Mass , 1984

Sample, J.C., M.R. Reid, H.J. Tobin, and J.C Moore, Carbonate cements indicate channeled fluid flow along a zone of vertical faults at the deformation front of the Cascadia accretionary wedge, *Geology, 21*, 507-510, 1993.

Scheidegger, K.F., Thermal evolution of the Juan de Fuca plate, in *Western North American Continental Margin and Adjacent Ocean Floor off Oregon and Washington, Ocean Margin Drill. Prog. Reg. Atlas Ser.*, atlas 1, edited by L.D. Kulm, sheet 8, Mar. Sci. Int., Woods Hole, Mass , 1984.

Scholtz, C.H., and C. Small, The effect of seamount subduction on seismic coupling, *Geology, 25*, 487-490, 1997.

Shrieve, R.L., and M. Cloos, Dynamics of sediment subduction, melange formation, and prism accretion, *J. Geophys. Res., 91*, 10,229-10,245, 1986.

Simpson, R.W , and A. Cox, Paleomagnetic evidence for tectonic rotation of the Oregon Coast Range, *Geology, 5*, 585-589, 1977.

Snavely, P.D., Jr., Tertiary geologic framework, neotectonics, and petroleum potential of the Oregon-Washington continental margin, in *Geology and Resource Potential of the Continental Margin of Western North America and Adjacent Ocean Basins: Beaufort Sea to Baja California, Earth Sci Ser*, vol. 6, edited by D.W. Scholl, A. Grantz, and J.G. Vedder, J.G., pp 305-335, Circum-Pac. Counc. for Energy and Miner. Resour., Houston, Tex., 1987.

Snavely, P.D., and R E. Wells, Cenozoic evolution of the continental margin of Oregon and Washington, in *Assessing Earthquake Hazards and Reducing Risk in the Pacific Northwest*, edited by A M. Rogers, *U.S. Geol. Surv. Prof Pap , 1560*, 161-182, 1996.

Snavely, P.D., Jr., N.S. MacLeod, and H.C. Wagner, Tholeiitic and alkalic basalts of the Eocene Siletz River volcanics, Oregon Coast Range, *Am. J. Sci., 266*, 454-481, 1968.

Snavely, P D., Jr., H.C. Wagner, D.L. Lander, Geologic cross section of the central Oregon continental margin, report, Plate Tecton. Group, U.S. Geodyn. Comm., Geol. Soc. of Am., Boulder, Colo., 1980.

Snavely, P D., Jr., H.C. Wagner, D.L. Lander, Land-sea geologic cross section of the southern Oregon continental margin, *U S Geol. Surv. Misc. Invest. Ser. Map, I-1463*, 1985

Tabor, R.W., R.S. Yeats, and M L Sorensen, Geologic map of the Mount Angeles quadrangle, Clallam and Jefferson counties, WA, *U. S Geol. Surv. Map, GQ-958*, 1972.

Talwani, M., and J.R. Heirtzler, Computation of magnetic anomalies caused by two-dimensional bodies of arbitrary shape, in *Computers in the Mineral Industries*, vol. 9, part 1, edited by G.A. Parks, pp. 464-480, Stanford Univ. Press, Stanford, Calif , 1964.

Talwani, M , J.L. Worzel, and M. Landisman, Rapid gravity computations for two-dimensional bodies with application to the Mendocino submarine fracture zone, *J. Geophys. Res.*, 64, 49-59, 1959.

Telford, W.M., L.P. Geldart, R.E. Sheriff, *Applied Geophysics*, 770 pp., Cambridge Univ. Press, New York, 1990.

Tréhu, A.M , I. Asudeh, T.M. Brocher, J.H. Luetgert, W.D. Mooney, J.L. Nabelek, and Y. Nakamura, Crustal architecture of the Cascadia forearc, *Science, 265*, 237-243, 1994.

Tréhu, A.M., G Lin, E. Maxwell, C Goldfinger, A seismic reflection profile across the Cascadia subduction zone offshore central Oregon: New constraints on methane distribution and crustal structure, *J. Geophys. Res., 100*, 15,101-15,116, 1995

U.S. Geological Survey, Aeromagnetic survey composite map, Oregon coast, *U.S. Geol. Surv. Open File Rep.*, 70-341, 1970.

von Huene, R., and D. Scholl, Observations at convergent margins concerning sediment subduction, subduction erosion, and the growth of continental crust, *Rev. Geophys., 29*, 279-316, 1991.

von Huene, R., I.A. Pecher, M.-A. Gutscher, Development of the accretionary prism along Peru and material flux after subduction of Nazca Ridge, *Tectonics, 15*, 19-33, 1996.

Wang, K., Simplified analysis of horizontal stresses in a buttressed forearc sliver at an oblique subduction zone, *Geophys. Res. Lett., 23*, 2021-2024, 1996.

Wang, W -H., and D.M. Davis, Sandbox model simulation of forearc evolution and noncritical wedges, *J Geophys. Res , 101*, 11,329-11,339, 1996

Weaver, C.S., and K.M. Shedlock, Estimates of seismic source regions from the earthquake distribution and regional tectonics in the Pacific northwest, in *Assessing Earthquake Hazards and Reducing Risk in the Pacific Northwest*, edited by A.M. Rogers, *U.S. Geol. Surv. Prof. Pap., 1560*, 161-182, 1996.

Webring, M., SAKI: A fortran program for generalized linear inversion of gravity and magnetic profiles, *U.S. Geol. Surv. Open File Rep. 85-122*, 1985.

Wells, R.E , D.C. Engebretson, P D. Snavely Jr., and R.S. Coe, Cenozoic plate motions and the volcano-tectonic evolution of western Oregon and Washington, *Tectonics, 3*, 275-294, 1984.

Wells, R.E., C.S. Weaver, and R.J. Blakely, Fore-arc migration in Cascadia and its neotectonic significance, *Geology, 26*, 759-762, 1998

Werner, K.S., E.P. Graven, T.A. Berkman, M.J Parker, Direction of maximum horizontal compression in western Oregon determined by borehole breakouts, *Tectonics, 10*, 948-958, 1991.

Wessel, P., and W.H.F. Smith, Free software helps map and display data, *Eos Trans. AGU, 72*, 441, 1991.

Wilson, D.S., Confidence intervals for motion and deformation of the Juan de Fuca plate, *J. Geophys. Res., 98*, 16,053-16,071, 1993.

Yeats, R. S., L.D. Kulm, C. Goldfinger, L.C McNeill, Stonewall anticline: An active fold on the Oregon continental shelf, *GSA Bull , 110*, 572-587, 1998.

Zelt, C.A., and R.S. Smith, Seismic travel-time inversion for 2-D crustal velocity structure, *Geophys. J. Int., 108*, 16-34, 1992.

S. W. Fleming, 204-620 Dobson Road, Duncan, British Columbia, Canada V9L 4R8.

A M. Tréhu, College of Oceanic and Atmospheric Sciences, Oregon State University, 104 Ocean Administration Bldg., Corvallis, OR 97331-5503. (trehu@oce.orst.edu)

(Received July 10, 1998; revised April 16, 1999,
accepted April 27, 1999.)